

Atomic Gradiometers for Accuracy Enhancement of Heart Magnetic Fields Measurement

Maliheh Ranjbaran^a, Reza Sedeyan^b, Amin Zamani^b, Mohammad Mehdi Tehranchi^{b,c,*},
Seyed Mohammad Hosein Khalkhali^d, and Seyedeh Mehri Hamidi^b

^aDepartment of Physics, Central Tehran Branch, Islamic Azad University, Tehran, Iran

^bLaser and Plasma Research Institute, Shahid Beheshti University, Tehran, Iran

^cPhysics Department, Shahid Beheshti University, Tehran, Iran

^dDepartment of Physics, Kharazmi University, Tehran, Iran

Corresponding author email: Teranchi@sbu.ac.ir

Regular Paper-Received: Mar. 01, 2024, Revised: June 19, 2024, Accepted: June 21, 2024, Available Online: June 23, 2024,
DOI: 10.61186/ijop.17.2.155

Abstract— the measurement of magnetic field generated by heart activity is crucial for the diagnosis and treatment of heart diseases and failures. Atomic magnetometers are an excellent choice for detecting bio-magnetic fields due to their comparable sensitivity to superconducting quantum interference devices, lower manufacturing costs, and lack of requirement for low temperatures. These magnetometers detect the magnetic field resulting from heart activity by measuring the Zeeman energy splitting and changes in laser light intensity as it passes through an alkali metal vapor cell. To improve the sensitivity of the measurements, this study presents a gradiometer design that utilizes two atomic magnetometers to eliminate environmental magnetic noise. By using a derivative technique, the homogeneous noises in both magnetometer channels are effectively eliminated. The gradiometer is capable of detecting the magnetic field produced by a frog's heart with a sensitivity of $860 \text{ fT}/\sqrt{\text{Hz}}$ even without magnetic shielding and in the presence of the Earth's field. This gradiometer design can be expanded to include multiple channels for mapping the heart's magnetic field.

Keywords: Atomic magnetometer, Biomagnetism, Gradiometer, Noise cancellation, Zeeman splitting detection.

I. INTRODUCTION

Electrocardiography (ECG) is pivotal for detecting the heart's electrical signals and is widely applied in clinical settings [1,2].

However, Magnetocardiography (MCG) offers a non-invasive method to measure variations in magnetic field strength above the thorax, allowing for the detection and analysis of the heart activity including the timing, rhythm, and strength of its contractions [3,4]. Various magnetic sensors, including superconducting quantum interference devices (SQUIDs) [2], tunneling magnetoresistance (TMR) sensors [5], and optically pumped magnetometers (OPMs), have been utilized for MCG measurements.

Despite advancements in SQUIDs techniques, which have improved MCG sensitivity, their reliance on cryogenic operations results in bulky and costly systems [6]. To address these limitations, low-cost atomic magnetometers operating at room temperature, while maintaining sensitivity comparable to SQUIDs, have garnered attention. Many of these atomic magnetometers, utilizing alkali metal vapors, operate close to zero fields in a spin-exchange relaxation-free (SERF) regime [7]. However, they still require magnetic shielding to mitigate the influence of the Earth's magnetic field, necessitating operation in a very low magnetic field [8], [9]. Numerous studies have demonstrated the potential superiority of MCG over ECG for certain clinical applications [10], [11].

MCG has been found to be more accurate than ECG in diagnosing conditions such as right atrial hypertrophy and right ventricular hypertrophy. It has also been used to non-invasively determine the location of conduction pathways in the heart, potentially aiding in the localization of arrhythmia sources for catheter ablation [12-14]. Moreover, MCG has proven useful in identifying spatial current dispersion patterns, characterizing and distinguishing Brugada syndrome, and completing the right bundle branch block [15].

Additionally, MCG can detect circular vortex currents that do not produce an ECG signal, potentially offering better or different insights into ischemia-induced deviations from normal depolarization and repolarization directions compared to ECGs. From a clinical perspective, MCG offers significant advantages over ECG [16]. It allows for the collection of electrophysiological waveforms without physical contact between the device and the patient, avoiding problems associated with skin-electrode contact encountered in ECG [17]. Moreover, MCGs offer the potential to offer more insights compared to ECGs. They achieve this by capturing the local magnetic field generated by both intracellular and extracellular currents (flow of electrical charges within the individual cells) in the heart tissue. In contrast, ECGs solely pick up on the effects of currents circulating through the body tissue (overall electrical activity of the entire tissue) [3], [18]-[20].

The QT interval includes the Q wave, the R wave, and the T wave on an ECG tracing. It is an important parameter in assessing the electrical activity of the heart and can provide information about the duration of ventricular depolarization and repolarization. Although the clinical significance of electrical QT wave dispersion from the electrocardiogram remains uncertain, multichannel MCGs may enable a more sensitive calculation of the cellular dispersion of ventricular repolarization. This is due to inherent differences between electric and magnetic cardiac fields. Such differences allow for the identification of regional as well as global variations in repolarization [21].

Dispersion information from electrocardiography is limited because the current flow from any single localized region produces an ECG effect at almost any body surface location. Additionally, discontinuities in the electric conductivity of body tissues like fat layers or bones act as spatial low-pass filters, and the available information on ventricular recovery times is primarily influenced by maximum repolarization time and less by local inhomogeneities [22]. This is not the case for magnetic signals [23],[24]. Many of the published studies suggest the potential value of MCG [25]-[27].

Tsukada pioneered the construction of the first multi-channel SQUID system for measuring cardiac magnetic fields, in 1991, [28]. In 2009, Bison unveiled a room-temperature 19-channel adult MCG imaging system utilizing optical double-resonance Caesium (Cs) vapour magnetometers within an eddy-current shield. Despite the inclusion of a paraffin-coated 30 mm glass cell, this configuration's sensitivity was capped at $300 \text{ fT}/\sqrt{\text{Hz}}$ [29]. By 2012, Wyllie had developed a dual-beam SERF AM array for adult MCG measurements, comprising four individual magnetometer modules with a channel spacing of 7 cm [6, 30]. In 2018, a research team from Nottingham University harnessed an array featuring 13 single-beam magnetometers by QuSpin, achieving magnetoencephalography (MEG) of brain activity surpassing the spatial resolution of cryogenic systems [10]. Presently, the QuSpin Gen-3 OPM boasts a compact volume of approximately 5cm^3 .

This research introduces a novel approach for magnetocardiography in environments lacking magnetic shielding, utilizing a gradiometric method with two rubidium alkali metal vapor cells. This method enables the detection of cardiac magnetic signals amidst the Earth's magnetic field and surrounding magnetic noises. The efficacy of this gradiometer is demonstrated through measurements of the frog's cardiac magnetic field in the absence of magnetic shielding.

II. METHODS

A. M_x Theory

Atomic magnetometers in M_x configuration operate by measuring the Larmor frequency of spin polarization within an alkali metal vapor when exposed to a magnetic field. When an alkali metal atom interacts with a magnetic field, it experiences torque on its angular momentum, causing it to precess around the magnetic field at a frequency known as the Larmor frequency. This precession occurs orthogonally to the direction of the magnetic field. By detecting this frequency, the applied magnetic field can be quantified [7].

From a quantum perspective, this phenomenon can be explained as the manifestation of Zeeman splitting caused by the external magnetic field. When the atom is exposed to the magnetic field, the hyperfine energy levels of the atom are split into Zeeman sublevels. Optical pumping techniques are then used to align the spins of the atoms with the highest level of the ground state. Subsequently, an oscillating radiofrequency magnetic field is applied to create coherence in the atom's polarization. Coherence is achieved when the energy of the oscillating magnetic field matches the energy difference due to Zeeman splitting ($E = \hbar\omega$), where ω represents the Larmor frequency ($\omega_1 = \gamma B$), which is directly proportional to the strength of the applied magnetic field B [31],[32].

B. Gradiometer Theory

To address the challenges such as mitigating the influence of the Earth's magnetic field and environmental noise in the sensitive magnetometer measurements, employing magnetic gradiometry is a beneficial technique. Gradiometry involves using two closely positioned magnetometers to compare signals and enhance sensitivity while reducing noise.

In the context of biomagnetic measurements like magnetocardiography, where precise and accurate readings are crucial, gradiometry helps in improving the signal-to-noise ratio. By comparing the signals from the two magnetometers at a specific separation distance

(as shown in Fig. 1), the technique allows for the differentiation between the desired signal and unwanted noise or interference. Implementing gradiometry in magnetometer setups can help in effectively isolating the desired biomagnetic signals from background noise, thereby improving the overall accuracy of measurements in unshielded environments.

Minimizing homogeneous noises between the two channels is an effective approach to improve the signal-to-noise ratio in this configuration. In contrast to standalone magnetometers, magnetic gradiometers indeed offer a superior signal-to-noise ratio. This advantage makes them particularly well-suited for detecting and measuring weak magnetic field sources in various applications [33, 34].

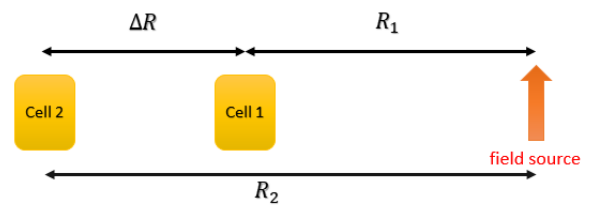


Fig. 1. Structure of magnetic gradiometer.

In this gradiometer configuration, M_x atomic magnetometers are employed, with two rubidium alkali metal cells positioned 5 cm apart to measure the field variance. A Helmholtz coil is used to produce a radio frequency (RF) field within both cells. The magnetometers are operated in a phase-locked mode, synchronized with a common RF control across the sensor cells. This synchronization ensures that the Larmor frequency of the atomic moments aligns with the RF frequency in both sensors, facilitating the concurrent correction of uniform ambient field fluctuations in both channels.

The operation of the gradiometer can be explained as shown in Fig. 1. The output signal, S_i , representing the signal of each magnetometer, is expressed as $S_i = M_i B(R_i)$, where M_i is the response function of the magnetometer to the applied magnetic field, and $B(R_i)$ denotes the magnetic field amplitude at distance R_i from the source. The gradiometric signal, S_G , representing the difference between

the two fields obtained from the magnetometer signals, is computed using Eq. 1.

$$S_G = S_1 - S_2 = M_1 B(R_1) - M_2 B(R_2) \quad (1)$$

The symbol ΔR represents the distance between the two cells, set at $\Delta R = 5$ cm. This configuration enables the gradiometer to effectively eliminate the background noise, thereby enhancing sensitivity [33].

III. EXPERIMENTAL SETUP

The magnetic gradiometer setup, depicted in Fig. 2, comprises two cubic rubidium alkali vapor cells (^{87}Rb isotope) with dimensions of $15 \times 10 \times 10$ mm³ positioned 5 cm apart. Electrical Heaters are employed to vaporize the rubidium within the cells. Spin polarization of the Rubidium atom is achieved using a 794.8 nm laser, set to $F=3 \rightarrow F'=2$ hyperfine transition of the D_1 absorption line of rubidium.

To facilitate optical pumping, the initial step involves the laser light passing through a polarizer and a quarter-wave plate ($\lambda/4$) arranged at a 45-degree angle to each other. This configuration results in circular polarization of the laser light. Then, the laser beam encounters a 50/50 beam splitter, which divides the beam into two separate beams of equal intensity. Each of these beams then passes through their respective vapor cells.

Circular Helmholtz coils, positioned adjacent to each cell and perpendicular to the applied magnetic field direction, induce an RF field. This RF field prompts the spins precession around the fixed magnetic field, known as spin resonance. To nullify the influence of the Earth's magnetic field, three pairs of orthogonal Helmholtz coils are utilized [7,33].

Subsequently, the oscillating radio frequency (RF) field is finely tuned near the Larmor frequency utilizing a frequency sweeper. Changes in the light intensity passing through the cells are then detected by recording both the in-phase and out-of-phase components of a

Lock-in amplifier and a computer equipped with Laboratory Virtual Instrument Engineering Workbench (LabVIEW) software. The resonance frequency is then determined from the recorded signals.

After optimizing the RF field amplitude, and the laser pump intensity [32], the detectors signals are differentially subtracted across two channels. This process facilitates the measurement of the field gradient and so the removal of background noise.

IV. RESULTS AND DISCUSSION

Initially, a constant current is applied to the three-axis Helmholtz coils to attenuate the Earth's magnetic field, resulting in the generation of a near-zero magnetic field at the center of both cells along the x-axis. Subsequently, variations in laser light intensity passing through the two cells, by sweeping the frequency of the oscillating RF field around the Larmor frequency, are recorded. The resulting intensity signals are then routed to a lock-in amplifier via two optical detectors and subsequently recorded by a computer.

In Fig. 3, the resonance signals from each channel of the gradiometer are shown. When the cells are exposed to the RF field, they absorb energy resonantly, causing the in-phase component of the signal to exhibit a Lorentzian pattern around the Larmor frequency. The out-of-phase component displays a distinct peak and valley pattern. It is worth noting that the inflection point at 1650 Hz in the phase diagram aligns with the resonance frequency of the cells, suggesting a decrease in background magnetic fields to 366 nT.

For precise measurement of weak magnetic fields using the gradiometric technique, it's essential that the resonance frequencies in both measurement channels are closely matched.

Additionally, to enhance the sensitivity of gradiometer, it's important that the resonance signals in both channels exhibit (the resonance signals in both channels must exhibit) a comparable ratio of width to amplitude.

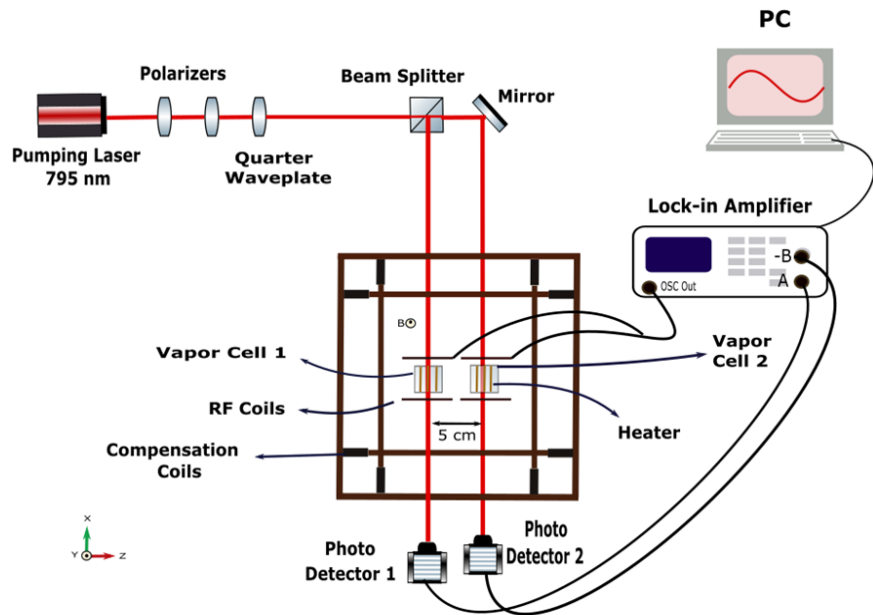


Fig. 2. Magnetic gradiometer setup for frog heart signal recording.

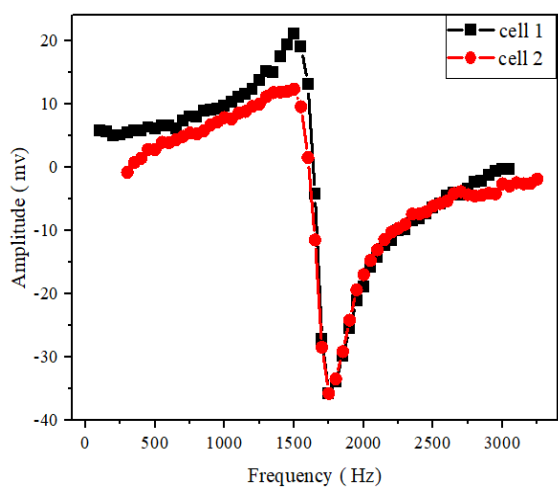


Fig. 3. Out-of-phase component of resonance signal at two channels of gradiometer.

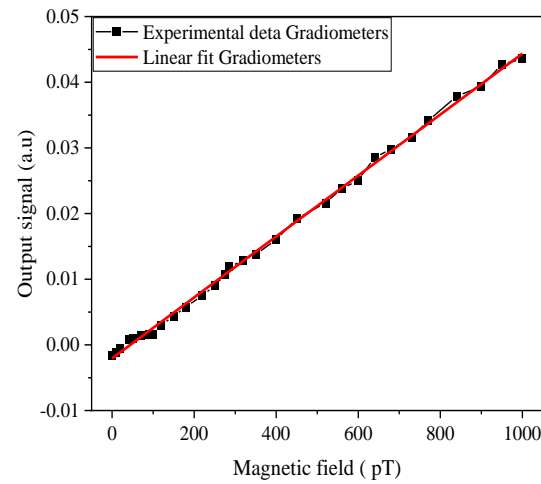


Fig. 4. The linear input-output relationship of the gradiometer.

To demonstrate the gradiometer's ability to accurately detect and measure magnetic field variations, its linearity is measured. Linearity is typically obtained by applying a known magnetic field input to the gradiometer and observing the corresponding output signal response at a specific frequency. Fig. 4. indicates remarkable linearity. A highly linear OPM will provide a consistent and reliable output signal that directly corresponds to changes in the magnetic field, such as heart magnetic field.

Given that the gradiometer exhibits distinct responses to magnetic fields with different frequencies, it is essential to evaluate its frequency response to enhance its performance. To investigate this aspect, we have adjusted the frequency of the sinusoidal input signal within the specific low-frequency range relevant to cardio-magnetic research, swept from 1 to 40 Hz. The frequency response of the gradiometer is plotted as the input-output ratio in Fig. 5. In this Figure, overall decrease at higher frequencies can be seen in the response of the magnetometer due to limitations in the measurement system's ability to accurately track and measure the input signal.

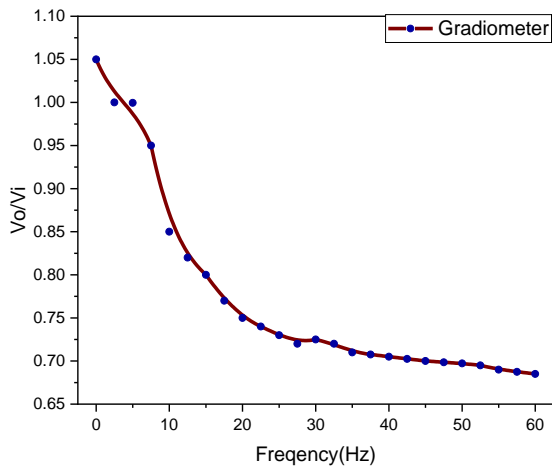


Fig. 5. Experimental frequency response of the gradiometers (output to input ratio as a function of applied magnetic field frequency).

Before recording the weak magnetic field emanating from the frog's heart, it is essential to accurately characterize noise in the magnetometer system. To accurately quantify the noise characteristics of the magnetometer, typically the noise spectral density, often expressed in units of $V/\sqrt{\text{Hz}}$ in power mode, was measured. This measurement helped in understanding the noise present in the system within a specific frequency range of interest, especially at the Larmor frequency.

To determine the spectral noise density, Fourier transformation of the data has been used. This process allowed analysis of the noise characteristics at various frequencies, which is crucial for ensuring accurate measurements of weak magnetic fields [34],[35]. As illustrated in Fig. 6, the gradiometer demonstrates a sensitivity of approximately $860 \text{ fT}/\sqrt{\text{Hz}}$ within the unshielded environment.

Following the characterization of spectral density and the establishment of the gradiometer's sensitivity, the oscillating field frequency is precisely locked onto the Larmor frequency as determined from the resonance curve. Subsequently, to record the magnetic signal originating from the frog's heart, the frog is brought into proximity of the gradiometer within an open-air laboratory environment.

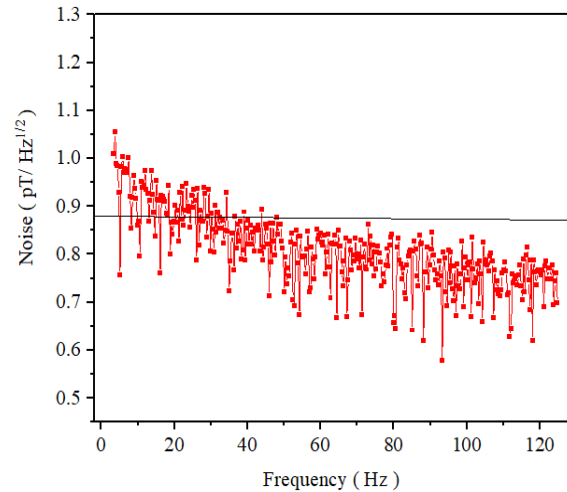


Fig. 6. Spectral noise density of the gradiometer without magnetic shielding.

The resulting signal, reflecting the magnetic field generated by the frog's heartbeat, is depicted in Fig. 7. It's evident that the gradiometer adeptly tracks and captures the signal stemming from the frog's cardiac activity, underscoring its efficacy in detecting biological magnetic fields.

The analysis and interpretation of the MCG signal should consider frequencies ranging from DC up to 40 Hz [36]. This frequency range is crucial for capturing the relevant information embedded in the MCG signal related to the heart's electrical activity. From Fig. 6. It is obvious that the sensitivity of the gradiometer, is approximately $860 \text{ fT}/\sqrt{\text{Hz}}$, within this frequency range.

For interpreting the MCG signal obtained from a frog's heart, we can use a similar approach to interpreting an ECG signal acquired in other research studies [37], [38], which includes the P wave, QRS complex, and T wave. The obtained signal is in good agreement with

The PQRST complex of the heart reflects the sequential depolarization and repolarization of the cardiac cells during each heartbeat. Similar to mammalian hearts, the PQRST complex in frogs comprises distinct waves and intervals. The "P" wave represents atrial depolarization, indicating the contraction of the atria, while the "QRS" complex corresponds to ventricular depolarization, signaling the contraction of the ventricles. The "T" wave marks ventricular

repolarization, representing the relaxation phase of the ventricles. This sequence is fundamental for coordinating the rhythmic contraction and relaxation of the heart muscle, essential for efficient blood circulation throughout the frog's body.

By analyzing the timing, morphology, and amplitudes of these waveforms in the MCG signal, we can gain more insights into the electrical activity and function of the frog's heart. This information can help assess the heart's rhythm, conduction, and potential abnormalities.

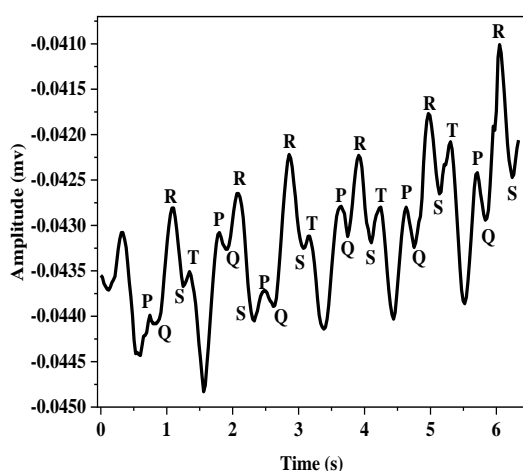


Fig. 7. Frog's heart MCG signal.

V. CONCLUSION

The magnetic fields arising from cardiac activity carry crucial diagnostic and therapeutic information regarding various heart conditions and failures. Atomic magnetometers offer sensitivity comparable to superconducting quantum interference devices (SQUIDs) while boasting cost-effective manufacturing and operation at room temperature, making them an optimal choice for biomagnetic field measurements.

To enhance the sensitivity of the gradiometer, it's imperative to mitigate homogeneous noise present in the two identical magnetometer channels. To address this challenge, the present research employs a gradiometric design aimed at suppressing unwanted magnetic noise. This gradiometer configuration comprises two atomic magnetometers.

Remarkably, the gradiometer successfully measures the magnetic field generated by the frog's heart even in environments lacking magnetic shielding and amidst the Earth's magnetic field. Achieving a sensitivity of 860 fT/ $\sqrt{\text{Hz}}$ within such unshielded spaces, the gradiometer effectively detects the magnetic fields emanating from the frog's heart.

The responses obtained from the gradiometer affirm its capability to accurately track changes in the magnetic field and reliably record the magnetic activity of the frog's heart. This underscores the gradiometer's potential in advancing the understanding and diagnosis of cardiac conditions through precise biomagnetic field measurements.

REFERENCES

- [1] H. Koch, "SQUID magnetocardiography: Status and perspectives," *J. IEEE Trans. Appl. Supercond.*, Vol. 11, pp. 49-59, 2001.
- [2] P.M. Vetoshko, N.A. Gusev, D.A. Chepurnova, E.V. Samoilova, I.I. Syvorotka, I.M. Syvorotka, and V.I. Belotelov. "Flux-gate magnetic field sensor based on yttrium iron garnet films for magnetocardiography investigations," *Tech. Phys. Lett.*, Vol. 42, pp. 860-864, 2016.
- [3] S. Morales, M.C. Corsi, W. Fourcalt, F. Bertrand, G. Cauffet, C. Gobbo, F. Alcouffe, F. Lenouvel, M. Le Prado, F. Berger, and G. Vanzetto, "Magnetocardiography measurements with ^4He vector optically pumped magnetometers at room temperature," *Phys. Med. Biol.*, Vol. 62, pp. 7267-1-12, 2017.
- [4] J.S. Kwong, B. Leithäuser, J.W. Park, and C.M. Yu. "Diagnostic value of magnetocardiography in coronary artery disease and cardiac arrhythmias: A review of clinical data," *Int. J. Cardiol.*, Vol. 167, pp. 1835-1842, 2013.
- [5] T. Inaba, Y. Nakazawa, K. Yoshida, Y. Kato, A. Hattori, T. Kimura, and K. Aonuma. "Routine clinical heart examinations using SQUID magnetocardiography at University of Tsukuba Hospital," *Supercond. Sci. Technol.*, Vol. 30, pp. 114003(1-6), 2017.
- [6] K. Fujiwara, M. Oogane, A. Kanno, M. Imada, J. Jono, T. Terauchi, and Y. Ando.

- “Magnetocardiography and magnetoencephalography measurements at room temperature using tunnel magneto-resistance sensors,” *Appl. Phys. Express*, Vol. 11, pp. 023001(1-4), 2018.
- [7] A. Zamani, M. Ranjbaran, M.M. Tehrani, S.M. Hamidi, and S.M.H. Khalkhali, “Myocardial Ischemia Detection by a Sensitive Pump-Probe Atomic Magnetometer,” *J. Lasers Med. Sci.*, Vol. 13, pp. 1-7, 2022.
- [8] R. Wyllie, M. Kauer, G.S. Smetana, R.T. Wakai, and T.G. Walker, “Magnetocardiography with a modular spin-exchange relaxation-free atomic magnetometer array,” *Phys. Med. Biol.*, Vol. 57, pp. 2619-2632, 2012.
- [9] E. Labyt, M.C. Corsi, W. Fourcault, A.P. Laloy, F. Bertrand, F. Lenouvel, G. Cauffet, M. Le Prado, F. Berger, and S. Morales, “Magnetoencephalography with optically pumped ^4He magnetometers at ambient temperature,” *IEEE Trans. Med.*, Vol. 38, pp. 90-98, 2018.
- [10] H. Cook, Y. Bezsudnova, L.M. Koponen, O. Jensen, G. Barontini, and A. Kowalczyk, “An optically pumped magnetic gradiometer for the detection of human biomagnetism,” *Quantum Sci. Technol.*, Vol. 2402, pp. 10113(1-7), 2024.
- [11] I.K. Kominis, T.W. Kornack, J.C. Allred, and M.V. Romalis, “A subfemtotesla multichannel atomic magnetometer,” *Nature*, Vol. 422, pp. 596-599, 2003.
- [12] H. Xia, A. Ben-Amar Baranga, D. Hoffman, and M.V. Romalis, “Magnetoencephalography with an atomic magnetometer,” *Appl. Phys. Lett.*, Vol. 89, pp. 211104(1-3), 2006.
- [13] J. Sheng, S. Wan, Y. Sun, R. Dou, Y. Guo, K. Wei, K. He, J. Qin, and J.H. Gao, “Magnetoencephalography with a Cs-based high-sensitivity compact atomic magnetometer,” *Rev. Sci. Instrum.*, Vol. 88, pp. 094304(1-5), 2017.
- [14] E. Boto, N. Holmes, J. Leggett, G. Roberts, V. Shah, S.S. Meyer, L.D. Muñoz, K.J. Mullinger, T.M. Tierney, S. Bestmann, and G.R. Barnes, “Moving magnetoencephalography towards real-world applications with a wearable system,” *Nature*, Vol. 555, pp. 657-661, 2018.
- [15] R.M. Hill, E. Boto, N. Holmes, C. Hartley, Z.A. Seedat, J. Leggett, G. Roberts, V. Shah, T.M. Tierney, M.W. Woolrich, and C.J. Stagg, “A tool for functional brain imaging with lifespan compliance,” *Nat. Commun.*, Vol. 10, pp. 4785(1-11), 2019.
- [16] R. Li, W. Quan, W. Fan, L. Xing, Z. Wang, Y. Zhai, and J. Fang, “A dual-axis, high-sensitivity atomic magnetometer,” *Chin. Phys. B*, Vol. 26, pp. 120702(1-5), 2017.
- [17] Z. Yuan, Y. Liu, M. Xiang, Y. Gao, Y. Suo, M. Ye, and Y. Zhai, “Compact multi-channel optically pumped magnetometer for bio-magnetic field imaging,” *Opt. Laser Technol.*, Vol. 164, pp. 109534(1-4), 2023.
- [18] K. Jensen, M.A. Skarsfeldt, H. Stærkind, J. Arnbak, M.V. Balabas, S.P. Olesen, and E.S. Polzik, “Magnetocardiography on an isolated animal heart with a room-temperature optically pumped magnetometer,” *Sci. Rep.*, Vol. 8, pp. 16218(1-9), 2018.
- [19] A. Kandori, W. Shimizu, M. Yokokawa, T. Noda, S. Kamakura, and K. Miyatake, “Identifying patterns of spatial current dispersion that characterise and separate the Brugada syndrome and complete right-bundle branch block,” *Med. Biol. Eng. Comput.*, Vol. 42, pp. 236-244, 2004.
- [20] H. Hañninen, P. Takala, M. Ma’kija’rvi, J. Montonen, P. Korhonen, and L. Oikarinen, “Recording locations in multichannel magnetocardiography and body surface potential mapping sensitive for regional exercise-induced myocardial ischemia,” *Basic Res. Cardiol.*, Vol. 96, pp. 405-414, 2001.
- [21] F.E. Smith, P. Langley, P. Van Leeuwen, B. Hailer, L. Trahms, U. Steinhoff, and A. Murray, “Comparison of magnetocardiography and electrocardiography: a study of automatic measurement of dispersion of ventricular repolarization,” *Europace*, Vol. 8, pp. 887-893, 2006.
- [22] A. Kandori, T. Hosono, Y. Chiba, M. Shinto, S. Miyashita, and M. Murakami, “Classifying cases of fetal Wolff–Parkinson–White syndrome by estimating the accessory pathway from fetal magnetocardiograms,” *Med. Biol. Eng. Comput.*, Vol. 41, pp. 33-39, 2003.
- [23] J.U. Sutter, O. Lewis, C. Robinson, A. McMahon, R. Boyce, R. Bragg, and E. Riis.

- "Recording the heartbeat of cattle using a gradiometer system of optically pumped magnetometers," *Comput. Electron. Agric.*, Vol. 177, pp. 105651(1-8), 2020.
- [24] H. Koch and W. Haberkorn, "Magnetic field mapping of cardiac electrophysiological function," *Philos. Trans. R. Soc. Lond.*, Vol. 359, pp. 1287-1298, 2001.
- [25] X. Han, X. Xue, Y. Yang, X. Liang, Y. Gao, M. Xiang, and X. Ning, "Magnetocardiography using optically pumped magnetometers array to detect acute myocardial infarction and premature ventricular contractions in dogs," *Phys. Med. Biol.*, Vol. 68, pp. 165006(1-6), 2023.
- [26] L.A. Bradshaw, R.S. Wijesinghe, and J.P. Wikswo, "Spatial filter approach for comparison of the forward and inverse problems of electroencephalography and magnetoencephalography," *Ann. Biomed. Eng.*, Vol. 29, pp. 214-226, 2001.
- [27] L.A. Bradshaw, W.O. Richards, and J.P. Wikswo, "Volume conductor effects on the spatial resolution of magnetic fields and electric potentials from gastrointestinal electrical activity," *Med. Biol. Eng. Comput.*, Vol. 39, pp. 35-43, 2001.
- [28] S. Dutz, M.E. Bellemann, U. Leder, and J. Haueisen, "Investigation of passive myocardial vortex currents in an anthropomorphic phantom," *Biomed. Tech.*, Vol. 48, pp. 230-231, 2003.
- [29] G. Bison, N. Castagna, A. Hofer, P. Knowles, J.L. Schenker, M. Kasprzak, H. Saudan, and A. Weis, "A room temperature 19-channel magnetic field mapping device for cardiac signals," *Appl. Phys. Lett.*, Vol. 95, pp. 173701(1-3), 2009.
- [30] R. Wyllie, M. Kauer, R.T. Wakai, and T.G. Walker, "Optical magnetometer array for fetal magnetocardiography," *Opt. Lett.*, Vol. 37, pp. 2247-2249, 2012.
- [31] M. Mosleh, M. Ranjbaran, S.M. Hamidi, and M.M. Tehranchi, "Ellipsometric spectroscopy of rubidium vapor cell at near-normal incidence," *Sci. Rep.*, Vol. 10, pp. 17080(1-9), 2020.
- [32] M. Ranjbaran, M.M. Tehranchi, S.M. Hamidi, and S.M.H. Khalkhali, "Harmonic detection of magnetic resonance for sensitivity improvement of optical atomic magnetometers," *J. Magn. Magn. Mater.*, Vol. 424, pp. 284-290, 2017.
- [33] I.A. Sulai, Z.J. DeLand, M.D. Bulatowicz, C.P. Wahl, R.T. Wakai, and T.G. Walker, "Characterizing atomic magnetic gradiometers for fetal magnetocardiography," *Rev. Sci. Instrum.*, Vol. 90, pp. 085003(1-10), 2019.
- [34] M.M. Tehranchi, R. Sedyan, M. Ranjbaran, S. M.H. Khalkhali, and S.M. Hamidi, "Atomic Gradiometer for Recording the Simulated Human Brain Signal in Unshielded Environment," *Int. J. Appl. Pharma.*, Vol. 14, pp. 40-51, 2024.
- [35] M. Ranjbaran, M.M. Tehranchi, S.M. Hamidi, and S.M.H. Khalkhali, "Relaxation time dependencies of optically detected magnetic resonance harmonics in highly sensitive Mx magnetometers," *J. Magn. Magn. Mater.*, Vol. 469, pp. 522-530, 2019.
- [36] G. Bison, R. Wynands, and A. Weis, "Dynamical mapping of the human cardiomagnetic field with a room-temperature, laser-optical sensor," *Opt. Express*, Vol. 11, pp. 904-909, 2003.
- [37] A. Bhaskar, A. Vinod, "Demonstration of the Origin of ECG," *Adv. Physiol. Educ.*, Vol. 30, pp. 128-128, 2006.
- [38] C.J. Ho and R.T. Ho, "The frog sign revisited," *J. Innov. Card. Rhythm. Manag.* Vol. 13, pp. 5184-5187, 2022.



Maliheh Ranjbaran received her M.Sc. and Ph.D. in photonics from the Laser and Plasma Research Institute, Shahid Beheshti University, Tehran, Iran, in 2010 and 2018, respectively. She is currently an assistant professor at the Central Tehran Branch of Azad University. Her research interests include biophotonics, magneto-photonics, design and modeling of optical systems, and optical measurement systems.



Reza Sedeyan received his B.Sc. in optics and laser engineering from Bonab University, Bonab, Iran, in 2019 and his M.Sc. in photonics from Shahid Beheshti University, Tehran, Iran, in 2023. He is currently working at Magneto-Photonic Lab., Shahid Beheshti University. His research interests include Photonics and their application in magnetometry and magneto-optics.



Amin Zamani received his B.Sc. in optics and laser engineering from Shahid Bahonar University, Kerman, Iran, in 2016 and his M.Sc. in photonics from Shahid Beheshti University, Tehran, Iran, in 2019. His research interests include optics, laser and their applications in magnetometry.



Mohammad Mehdi Tehranchi received his Ph.D. degree in physics from Prokhorov General Physics Institute of the Russian Academy of Sciences (GPI RAS) in 1997. He is currently a professor of physics and the director of the Magneto-Photonic Lab. of the

laser and plasma research Institute and the Physics Department of Shahid Beheshti University. He has worked on the research fields of magnetic materials (such as amorphous materials, multiferroic materials and magnetophotonic crystals) and magnetic effects (such as linear and nonlinear magneto-optical effects and Giant magnetoimpedance effects) which are utilized in magnetic sensors and nondestructive testing technology.



Seyed Mohammad Hossein Khalkhali received his Ph.D. degree in physics from the Physics Department of Shahid Beheshti University, Iran, in 2014. He is currently an assistant professor at Kharazmi University, Karaj, Iran. He has worked on the ferroelectric and photovoltaic composite thin films.



Seyedeh Mehri Hamidi received her Ph.D. degree in photonics from Laser and Plasma Research Institute, Shahid Beheshti University, Tehran, Iran, in 2009. She is currently the director of magneto-plasmonic Lab. of Laser and Plasma Research Institute. She has worked in the research fields of magneto-plasmonic, nanophotonics, photonic and magneto photonic crystals, surface plasmon resonance, dielectric and magnetic waveguides, and pulsed laser deposition technique.